Journal of Thermal Analysis and Calorimetry, Vol. 63 (2001) 533–547

CRYSTALLIZATION KINETICS OF $Pb_{20}Ge_{17}Se_{63}$ AND $Pb_{20}Ge_{22}Se_{58}$ CHALCOGENIDE GLASSES

M. M. Wakkad

Physics Department, Faculty of Science, South Valley University, Sohag, Egypt

(Received October 12, 2000)

Abstract

Two glasses of the chalcogenide system $Pb_{20}Ge_xSe_{80-x}$, with x=17 and 22 at.%, were prepared by the melt quench technique. Differential scanning calorimetry emphasized that the investigated $Pb_{20}Ge_{17}Se_{63}$ and $Pb_{20}Ge_{22}Se_{58}$ glasses are crystallized to $GeSe_2$ and $PbSe_2$ as well as $GeSe_2$ and PbSe, respectively as revealed by X-ray diffraction analysis. It was found that the glass transition temperatures of the $Pb_{20}Ge_{22}Se_{58}$ glass are higher than those of $Pb_{20}Ge_{17}Se_{63}$ ones. The respective values for the activation energy of glass transition (E_t) for $Pb_{20}Ge_{17}Se_{63}$ and $Pb_{20}Ge_{22}Se_{58}$ are found to be 434±20 and 761±77 kJ mol^{-1}, while those for the annealed samples are 928±85 and 508±23 kJ mol^{-1}, respectively. The activation energies of crystallization (E_c) before and after annealing were determined using different methods. Applying the modified Johnson–Mehl–Avrami (JMA) equation, it could be found that $GeSe_2$ is crystallized by surface crystallization, while both $PbSe_2$ and PbSe are crystallized by bulk crystallization in three dimensions.

Keywords: chalcogenide glasses, crystallization kinetics, differential scanning calorimetry, Pb–Ge–Se

Introduction

Chalcogenide glasses have attracted much attention in the field of electronics as well as infrared optics since they exhibit several peculiar phenomena, which are applicable for devices such as electrical switches and/or memory image storage and photoresistors [1–3]. It is generally recognized that most of the chalcogenide glasses show *p*-type conduction and their electrical conductivity is very slightly affected by doping. This insensitivity is attributed to the presence of charged defects, which pin the Fermi level near the midband gap [4]. Tohge *et al*. were the first to point out the role of Bi [5] and Pb [6] modifiers in the appearance of *n*-type conduction in germanium-chalcogenide glasses. Recently, notable investigations of the electronic conduction processes [7] and the phenomenon of carrier type reversal [8] in Pb–Ge–Se glasses were reported.

Structural studies of chalcogenide materials using various techniques are very important for better understanding of their transport mechanisms and thermal stabil-

1418–2874/2001/ $ 5.00

Akadémiai Kiadó, Budapest
Kluwer Academic Publishers, Dordrecht

ity. On the other hand, studies on the crystallization of a glass upon heating can be performed in several ways. In calorimetric measurements, two basic methods can be used, isothermal and non-isothermal. However, the results of crystallization process can be interpreted in terms of several theoretical models [9–11 and references therein].

The present work concerns studies on thermal stability, annealing effect and crystallization kinetics for the two-chalcogenide glasses, $Pb_{20}Ge_{17}Se_{63}$ and $Pb_{20}Ge_{22}Se_{58}$, as *p*-type and *n*-type semiconductors, respectively. The kinetic parameters of the glass-crystallization transformation were estimated under non-isothermal conditions applying three different approaches, namely, Kissinger [12], Augis and Bennett [13] and modified Johnson–Mehl–Avrami (JMA) [14].

Experimental procedures

Bulk chalcogenides $Pb_{20}Ge_{17}Se_{63}$ and $Pb_{20}Ge_{22}Se_{58}$ glasses were prepared by the melt quench technique as described in [6]. The glassy nature of the prepared bulk materials is confirmed by X-ray diffraction (XRD) patterns using X-ray diffractometer (Philips-1710), with Cu as a target and Ni as filter (λ=1.54178 Å), at 40 kV and 30 mA, with scanning speed 2° min^{-1}. For compositional determination by energy dispersive analysis of X-ray (EDAX), a scanning electron microscope (Cambridge-S 6000) and EDS unit (Link-AN 10000) were used.

A calibrated differential scanning calorimeter (DSC), (DuPont 2000), was used to obtain the thermal curves. The calorimetric sensitivity was 10 $\mu W\ cm^{-1}$ and the temperature precision was ±0.01 K. For each heating rate ϕ, ranging from 1.25 to 80 K min^{-1}, typically 20 mg of sample in powder form was sealed in standard aluminum pan and scanned from room temperature up to 813 K. High purity nitrogen was used as inert atmosphere. The values of glass transition temperature (T_g), the onset temperature of crystallization (T_c), the peak temperature of crystallization (T_p) and the melting temperature (T_m) were determined by using the microprocessor of the apparatus.

The fraction x crystallized at any temperature T is given as $x=A_T/A$, where A is the total area of the exotherm between the temperature T_s, where crystallization just begins, and the temperature T_e, where the crystallization is completed (Fig. 2), and A_T is the area between T_s and T as shown by the hatched portion on the lower DSC scan in Fig. 2.

Calculations of the average coordination number and the overall mean bond energy

The average coordination numbers Z of the studied glasses were evaluated using the standard procedure described by Tanaka [15], using coordination numbers (CN) of 4, 4 and 2 for Pb, Ge and Se, respectively. Thus, for the $Pb_xGe_ySe_z$ ($x+y+z=1$) glasses, the values of Z could be given by the following relation:

$$Z=xCN(\mathrm{Pb})+yCN(\mathrm{Ge})+zCN(\mathrm{Se}) \quad (1)$$

The bond energies (E_{AB}) of heteropolar A–B bonds can be, in first approximation, estimated using Pauling's relation [16]:

$$E_{AB}=0.5(E_{AA}+E_{BB})+23(X_A-X_B)^2 \quad (2)$$

where E_{AA} and E_{BB}, and X_A and X_B are, respectively, homopolar bond energies and electronegativity for *A* and *B* atoms. The homopolar bond energies and electronegativity are obtained from [17].

Values of the overall mean bond energy (<*E*>) for any glassy alloys, which were found [18] to depend on *Z*, the degree of cross-linking/atom (*P*), the type of bonds and the bond energy forming a network can be evaluated as described by Tichy and Ticha [18] using the following relation

$$<E>=E_c+E_{rm} \quad (3)$$

where $E_c=P_pE_{hp}$ is the mean bond energy of average cross-linking/atom; ($P_p=zCN(\mathrm{Se})/(x+y+z)$ is the degree of cross-linking/atom for the case of chalcogen-poor; $E_{hb}=[xCN(\mathrm{Pb})E_{Pb-Se}+yCN(\mathrm{Ge})E_{Ge-Se}]/[xCN(\mathrm{Pb})+yCN(\mathrm{Ge})]$ is the average heteropolar bond energy, where E_{Pb-Se} and E_{Ge-Se} are, respectively, the heteropolar bond energies of Pb–Se and Ge–Se heteropolar bonds); and E_{rm} is the average bond energy/atom of the 'remaining matrix' and for the present case (chalcogen-poor) can be written in the form

$$E_{rm}=\frac{2(0.5Z-P_p)E_{<>}}{Z}$$

where $E_{<>}=(E_{Pb-Pb}+E_{Ge-Ge}+E_{Pb-Ge})/3$ is the average bond energy of a 'metal–metal' bond in the chalcogen-poor region. Values of *Z* and <*E*> for the investigated glasses are listed in Table 1.

Table 1 Calculated values of *Z* and <*E*> for $Pb_{20}Ge_{17}Se_{63}$ and $Pb_{20}Ge_{22}Se_{58}$ glasses

Composition	*Z*	<*E*>/eV
$Pb_{20}Ge_{17}Se_{63}$	2.74	2.46
$Pb_{20}Ge_{22}Se_{58}$	2.84	2.49

Results and discussion

X-ray diffraction and phase transition temperatures

Figure 1 shows the X-ray diffractograms of the as-prepared $Pb_{20}Ge_{17}Se_{63}$ and $Pb_{20}Ge_{22}Se_{58}$ samples, confirming the glassy nature of their structure, together with the EDAX trace for the investigated glasses, where the percentage ratios of the elements in the prepared compositions are within ±2% of their nominal values.

A typical differential scanning calorimetry (DSC) thermal curves of the as-prepared $Pb_{20}Ge_{17}Se_{63}$ and $Pb_{20}Ge_{22}Se_{58}$ glasses as recorded at a heating rate of 10 K min^{-1} are shown in Fig. 2. The characteristic features of the investigated thermal

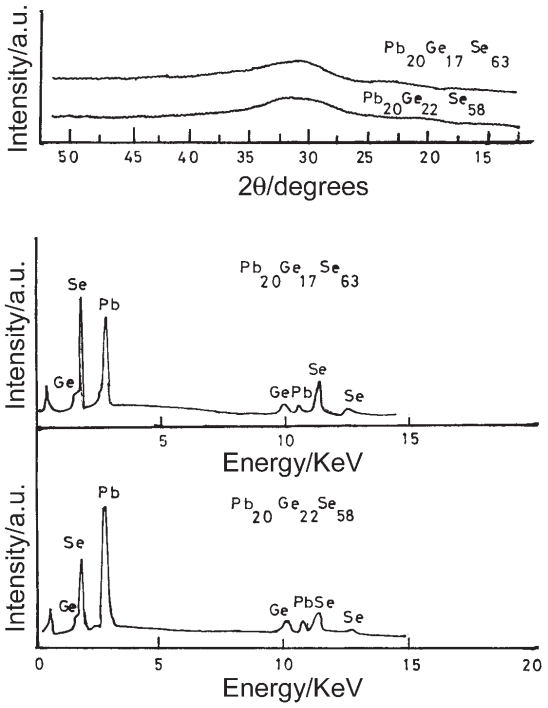

Fig. 1 X-ray diffractograms, a – and EDAX traces, b – of the as-prepared $Pb_{20}Ge_{17}Se_{63}$ and $Pb_{20}Ge_{22}Se_{58}$ materials

curves were as follows: Firstly, each one of the two glasses shows an endothermic step corresponding to its glass transition, at a temperature T_g. Secondly, the crystallization processes of each of the considered glasses show two exothermic crystallization peaks. Analysis of XRD, shown in Fig. 3, for samples successively annealed at temperatures corresponding to T_p of the observed phases, revealed that the $Pb_{20}Ge_{17}Se_{63}$ glass is crystallized in $GeSe_2$ and $PbSe_2$, whereas the $Pb_{20}Ge_{22}Se_{58}$ glass is crystallized in $GeSe_2$ and PbSe phases. Following the exothermic peak characterizing the crystallized phases, an endothermic peak due to melting at T_m of the glasses was observed. Values of the glass transition temperature (T_g), onset temperature of crystallization (T_c), peak temperature of crystallization (T_p) and the melting temperature (T_m) are given in Table 2 as a function of heating rate (ϕ). The table reveals that the values of T_g of $Pb_{20}Ge_{22}Se_{58}$ are higher than those of $Pb_{20}Ge_{17}Se_{63}$. This is related to the rigidity of the glass network, which is usually associated with the average coordination number and/or to the overall mean bond energy of the glass [18]. So, the obtained results may be attributed to a relatively higher value of the overall mean bond energy of $Pb_{20}Ge_{22}Se_{58}$ glass (2.49 eV) compared to that of $Pb_{20}Ge_{17}Se_{63}$ (2.46 eV).

Figure 4 shows typical DSC curves scanned at 10 K min^{-1} for $Pb_{20}Ge_{17}Se_{63}$ and $Pb_{20}Ge_{22}Se_{58}$ glasses annealed for 2 h at a temperature corresponding to the value of

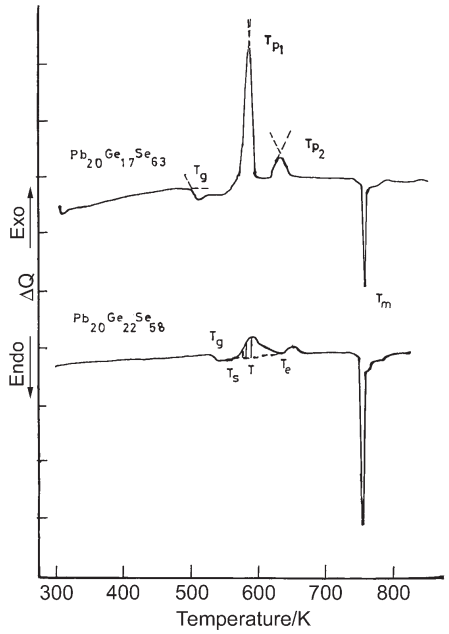

Fig. 2 Typical DSC thermal curves at heating rate ϕ=10 K min^{-1} for the as-prepared $Pb_{20}Ge_{17}Se_{63}$ and $Pb_{20}Ge_{22}Se_{58}$ chalcogenide glasses

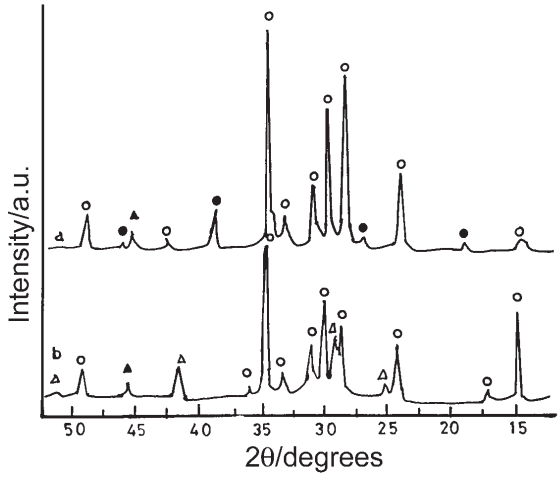

Fig. 3 X-ray diffractograms, a – annealed $Pb_{20}Ge_{17}Se_{63}$ at 601 K for 2 h and b – annealed $Pb_{20}Ge_{22}Se_{58}$ at 632 K for 2 h

T_{p1} for each composition (588 and 590 K, respectively). Table 3 summarizes the values of T_g and T_p as a function of ϕ for the annealed two glasses ($Pb_{20}Ge_{17}Se_{63}$–H and $Pb_{20}Ge_{22}Se_{58}$–H) investigated. The proper annealing of a glass at its T_{p1} temperature crystallizes its low temperature phase.

Table 2 Transition temperatures of as-prepared $Pb_{20}Ge_{17}Se_{63}$ and $Pb_{20}Ge_{22}Se_{58}$ glasses as a function of heating rates

Composition	$Pb_{20}Ge_{17}Se_{63}$					$Pb_{20}Ge_{22}Se_{58}$				
ϕ/K min^{-1}	T_g/K	T_c/K	T_{p1}/K	T_{p2}/K	T_m/K	T_g/K	T_c/K	T_{p1}/K	T_{p2}/K	T_m/K
1.25	492	562	570	601	754	525	562	581	632	756
2.5	495	567	575	610	755	525	568	586	637	756
5	497	573	582	623	756	528	572	588	641	756
10	501	578	588	638	756	529	575	590	651	756
20	504	582	594	651	758	531	582	596	659	759
40	509	588	600	676	760	533	590	606	668	762
80	511	589	611	680	762	537	598	617	679	765

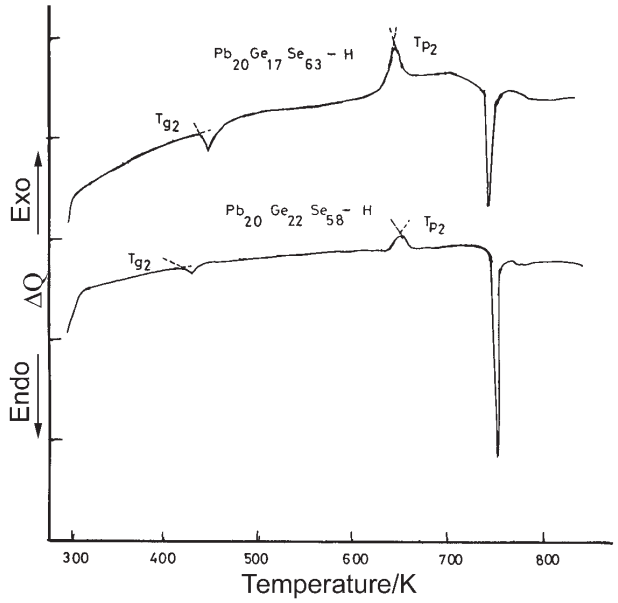

Fig. 4 Typical DSC thermal curves at heating rate ϕ=10 K min^{-1} for annealed $Pb_{20}Ge_{17}Se_{63}$ and $Pb_{20}Ge_{22}Se_{58}$ chalcogenide glasses at their T_{p1} for 2 h

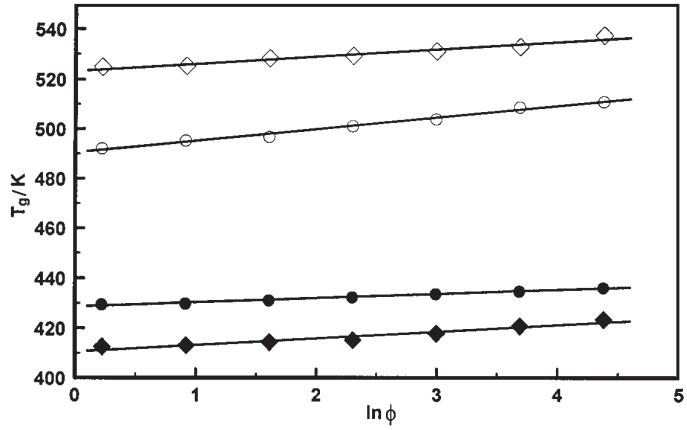

Fig. 5 Plots of T_g *vs.* lnϕ for as-prepared (o, ◊) and annealed (•, ♦) $Pb_{20}Ge_{17}Se_{63}$ and $Pb_{20}Ge_{22}Se_{58}$ chalcogenide glasses

Dependence of T_g on heating rate

To study the dependence of T_g on the heating rate one can use the following relation [19]

$$T_g = A + B\ln\phi \quad (4)$$

where A and B are constants for a given glass composition. Values of B determine the response of configurational changes within the glass transition region to the heating rate [19].

A plot of T_g *vs*. lnϕ for the as-prepared and annealed samples are shown in Fig. 5. The values of B were obtained from the figure using least square fit and listed in Table 4. However, all the recorded data of T_g and T_p *vs*. ϕ are best fitted by least square method. The values of the correlation coefficient for these results are in the range 0.92–0.99.

Table 3 Transition temperatures as a function of heating rates for annealed $Pb_{20}Ge_{17}Se_{63}$ and $Pb_{20}Ge_{22}Se_{58}$ glasses

Composition	$Pb_{20}Ge_{17}Se_{63}$–H			$Pb_{20}Ge_{22}Se_{58}$–H		
ϕ/K min^{-1}	T_{g2}/K	T_{p2}/K	T_m/K	T_{g2}/K	T_{p2}/K	T_m/K
1.25	429	598	748	413	631	750
2.5	430	608	750	413	638	752
5	431	622	753	414	646	753
10	432	637	757	415	652	756
20	434	656	758	418	663	759
40	435	678	762	421	670	761
80	436	704	763	423	680	766

Table 4 Values of B and E_t for as-prepared and annealed $Pb_{20}Ge_{17}Se_{63}$ and $Pb_{20}Ge_{22}Se_{58}$ glasses

Composition	B	E_t/kJ mol^{-1}
$Pb_{20}Ge_{17}Se_{63}$	4.68±0.22	434±20
$Pb_{20}Ge_{22}Se_{58}$	2.89±0.30	761±77
$Pb_{20}Ge_{17}Se_{63}$–H	1.65±0.07	928±85
$Pb_{20}Ge_{22}Se_{58}$–H	2.63±0.31	508±23

To determine the activation energy of glass transition (E_t) we considered the Kissinger formula [12], which is originally derived for the crystallization processes and suggested to be valid for glass transition [20]. This formula has the following form

$$\ln\frac{\phi}{T_g^2} = -\frac{E_t}{RT_g} + \text{const.} \quad (5)$$

where R is the universal gas constant.

The value of E_t is obtained from the slope of lnϕ/T_g^2 *vs*. $1/T_g$ plots given in Fig. 6 for the as-prepared and annealed samples. The calculated values of E_t are given in Table 4.

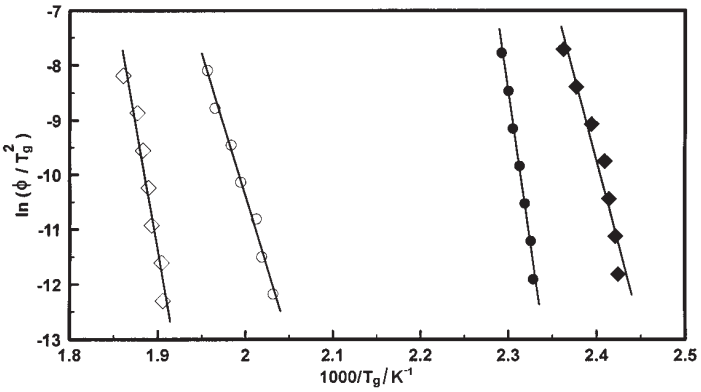

Fig. 6 Plots of $\ln(\phi/T_g^2)$ *vs.* $1000/T_g$ for as-prepared (o, ◊) and annealed (•, ♦) $Pb_{20}Ge_{17}Se_{63}$ and $Pb_{20}Ge_{22}Se_{58}$ chalcogenide glasses

Thermal stability and glass formation

A parameter usually employed to estimate the glass stability is the thermal stability (ΔT), which is defined by $\Delta T = T_c - T_g$ [21], where T_c is the onset temperature of crystallization. Another parameter introduced by Hruby and Stourac [22] is the glass forming ability (K_{g1}) which is defined by the relation

$$K_{g1} = \frac{T_c - T_g}{T_m - T_c} \tag{6}$$

Regarding T_g as the temperature at which the supercooled liquid hardens to a glass, the parameter K_{g1} stresses the fact that the probability of obtaining a glass increases as the supercooled interval $T_m - T_g$ decreases and its stability increases with the difference $T_c - T_g$. Good glass formers would, then, have high K_{g1}. The values of ΔT and K_{g1} have been calculated for the investigated glasses using the values of T_c and T_m at ϕ=10 K min^{-1} given in Table 2. The values of ΔT and K_{g1} are found to be 76.59 K and 0.43 as well as 45.43 K and 0.25 for the first phases of $Pb_{20}Ge_{17}Se_{63}$ and $Pb_{20}Ge_{22}Se_{58}$ glasses, respectively, while they are equal to 122.78 K and 0.93 as well as 109.55 K and 0.93 for the respective second phases. The resulting higher values of ΔT and K_{g1} obtained for the $Pb_{20}Ge_{17}Se_{63}$ glass compared to the other one can be related to its relatively lower overall mean bond energy in comparison with the other.

Activation energy of crystallization

The activation energy of crystallization (E_c) for the phases of the investigated glasses has been estimated using the following methods:

1. Kissinger's method [12], which relates the dependence of T_p on ϕ by the following equation

$$\ln\frac{\phi}{T_p^2}=-\frac{E_c}{RT_p}+\text{const.} \quad (7)$$

The value of E_c for the phases of as-prepared and annealed samples is obtained from the slope of $\ln(\phi/T_p^2)$ *vs.* $1/T_p$ plots given in Fig. 7.

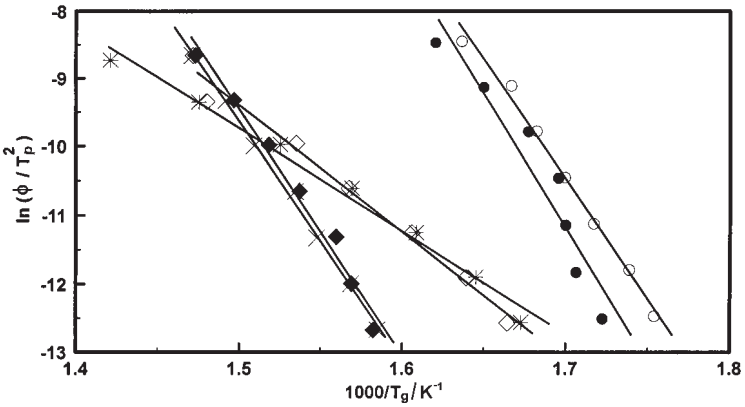

Fig. 7 Plots of $\ln(\phi/T_p^2)$ *vs.* $1000/T_p$ for the phases of $Pb_{20}Ge_{17}Se_{63}$ (o – $GeSe_2$ and ◊ – $PbSe_2$), $Pb_{20}Ge_{22}Se_{58}$ (● – $GeSe_2$, ♦ – PbSe), $Pb_{20}Ge_{17}Se_{63}$–H (* – $PbSe_2$) and $Pb_{20}Ge_{22}Se_{58}$–H (× – PbSe) chalcogenide glasses

2. Augis and Bennett's method [13], which gives the dependence of T_p on ϕ by the following form

$$\ln\left(\frac{\phi}{T_p-T_0}\right)=-\frac{E_c}{RT_p}+\text{const.} \quad (8)$$

where T_0 is the initial temperature (room temperature) of DSC thermal curves.

Plots of $\ln[\phi/(T_p-T_0)]$ *vs.* $1/T_p$ are shown in Fig. 8 that used to determine the values of E_c of the phases of the present glasses.

3.The modified Johnson–Mehl–Avrami (JMA) equation, which for non-isothermal kinetics the volume fraction x of crystals precipitated in a glass heated at a uniform rate ϕ is related to E_c through the expression [14]

$$\ln[-\ln(1-x)]=-n\ln\phi-1.052m\frac{E_c}{RT}+\text{const.} \quad (9)$$

where n and m are numerical factors depending on the nucleation process and growth morphology. When nuclei formed during the heating at constant rate are dominant, n is equal to $(m+1)$ and when nuclei formed in the previous heat treatment before thermal analysis run are dominant, n is equal to m [23]. The values of n and m are listed in Table 5, together with those of E_c, estimated according to Eqs (7), (8) and (9), for the glasses investigated.

Table 5 Crystallization kinetic parameters for the phases of the as-prepared and annealed $Pb_{20}Ge_{17}Se_{63}$ and $Pb_{20}Ge_{22}Se_{58}$ glasses

Composition	Phase	Eq. (7)	Eq. (8)	mE_c/	n	m	E_c/	$\overline{E}_c$/
		kJ mol^{-1}					kJ mol^{-1}	
$Pb_{20}Ge_{17}Se_{63}$	$GeSe_2$	293±12	292±12	505±18	1.49±0.16	1	505±18	292±12
$Pb_{20}Ge_{17}Se_{63}$	$PbSe_2$	154±9	154±9	804±27	3.85±0.28	3	268±9	154±9
$Pb_{20}Ge_{22}Se_{58}$	$GeSe_2$	326±45	326±45	551±20	1.44±0.15	1	551±7	326±45
$Pb_{20}Ge_{22}Se_{58}$	PbSe	298±18	299±18	1115±30	3.52±0.27	3	372±10	298±18
$Pb_{20}Ge_{17}Se_{63}$–H	$PbSe_2$	125±6	125±6	775±25	3.45±0.3	3	258±8	125±6
$Pb_{20}Ge_{22}Se_{58}$–H	PbSe	290±16	291±16	924±28	3.09±0.24	3	308±9	290±16

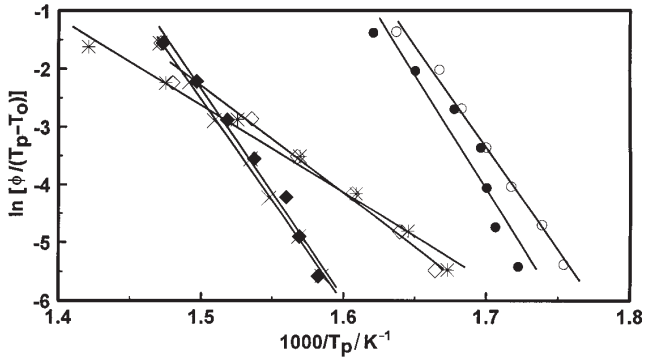

Fig. 8 Plots of $\ln[\phi/T_p-T_0)]$ *vs*. $1000/T_p$ for the phases of $Pb_{20}Ge_{17}Se_{63}$ (o – $GeSe_2$ and ◊ – $PbSe_2$), $Pb_{20}Ge_{22}Se_{58}$ (• – $GeSe_2$, ♦ – PbSe), $Pb_{20}Ge_{17}Se_{63}$–H (∗ – $PbSe_2$) and $Pb_{20}Ge_{22}Se_{58}$–H (× – PbSe) chalcogenide glasses

According to [9, 24], the cursory check of the JMA applicability to non-isothermal kinetics is the fractional extent of crystallization x at the maximum of relevant peak should be in the range 0.62–0.64 and it is only weakly dependent on the heating rate.

As an example, Figs 9a and b display the plot of $\ln[-\ln(1-x)]$ *vs*. $1/T$ at different heating rates (1.25–80 K min^{-1}) for the crystallization phases of the as-prepared $Pb_{20}Ge_{22}Se_{58}$ glass, where two distinct slopes can be noticed for each curve indicating saturation of nucleation sites in the final stages of crystallization [20] or restriction of crystal growth by the small size of the particles [25]. In all these cases, where there is a change in slope, the analysis is confined to the initial linear region [21]. The values of mE_c at different heating rates can be obtained from the slope of Fig. 9 and seemed to be slightly dependent on the heating rate. Therefore, the average values of mE_c were calculated and recorded in Table 5 for the phases of the $Pb_{20}Ge_{22}Se_{58}$ glass as well as for those calculated for $Pb_{20}Ge_{17}Se_{63}$, $Pb_{20}Ge_{17}Se_{63}$–H and $Pb_{20}Ge_{22}Se_{58}$–H glasses.

The data of Fig. 9 are used to evaluate $\ln[-\ln(1-x)]$ as a function of $\ln\phi$ for the two phases $GeSe_2$ and PbSe of the as-prepared $Pb_{20}Ge_{22}Se_{58}$ glass and are given in Fig. 10 at two different temperatures namely, 565 and 580 as well as 625 and 645 K. Similarly, the values of n have been evaluated for the phases of $Pb_{20}Ge_{17}Se_{63}$, $Pb_{20}Ge_{17}Se_{63}$–H and $Pb_{20}Ge_{22}Se_{58}$–H and the results are given in Table 5. For $Pb_{20}Ge_{17}Se_{63}$ and $Pb_{20}Ge_{22}Se_{58}$ glasses, no specific heat treatment was given before the DSC run to nucleate the samples, while $Pb_{20}Ge_{17}Se_{63}$–H and $Pb_{20}Ge_{22}Se_{58}$–H glasses are heat treated before the thermal run. Therefore, n is considered to be equal to $(m+1)$ for the former glasses and equal to m for the latter ones, [23]. Table 5 summarizes the values of m for all phases of the glasses considered.

Table 5 indicates that the crystallization process of $GeSe_2$ can be carried out by a surface crystallization, in consistent with the previously reported results [26, 27], while those of both $PbSe_2$ and PbSe by bulk crystallization in three-dimensions. Values of the activation energy of crystallization of all considered phases obtained by

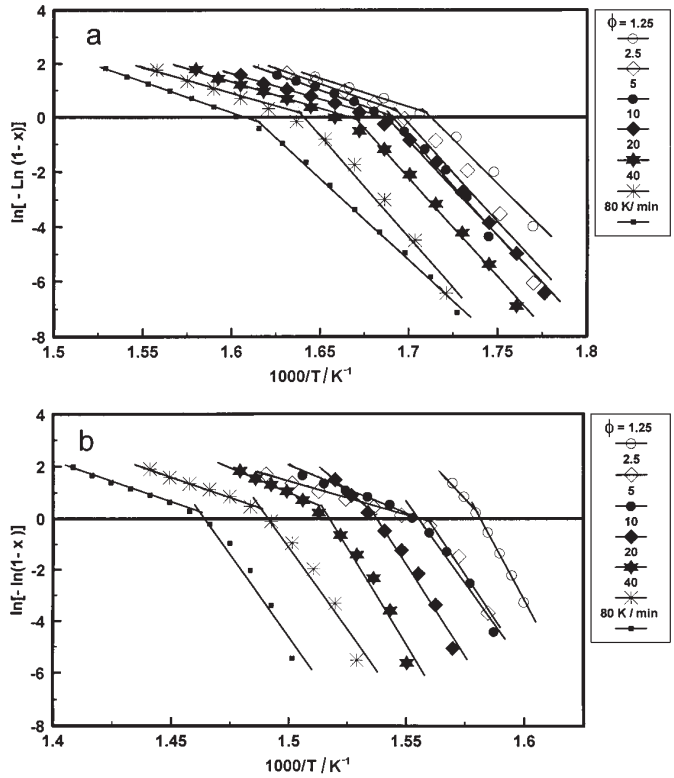

Fig. 9 Plots of ln[–ln(1–*x*)] *vs*. 1000/*T* for the phases of $Pb_{20}Ge_{22}Se_{58}$ (a – $GeSe_2$ and b – PbSe) chalcogenide glass at different heating rates

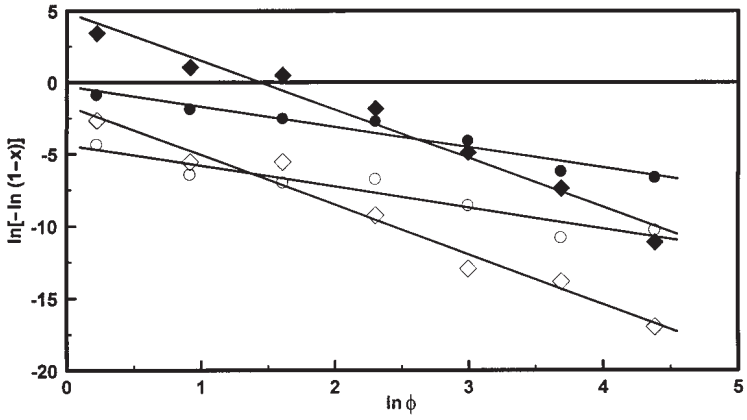

Fig. 10 Plots of ln[–ln(1–*x*)] *vs*. ln(ϕ) for the phases of $Pb_{20}Ge_{22}Se_{58}$ ($GeSe_2$; o – at 565 K and • – 580 K and PbSe; ◊ – at 625 K and ♦ –645 K) chalcogenide glass

both Kissinger and Augis–Bennett methods are confirming each other and so are accepted. However, these results are deviated much from those obtained by the modified JMA equation. This observation may be correlated to some deviation of our results from Handerson [9] and Malek [24] criterion of applicability of JMA equation to non-isothermal kinetics. Also, the mean values of the activation energy of crystallization ($\overline{E}_c$) calculated from the averaging of those obtained by methods of Kissinger and Augis–Bennett for $GeSe_2$ were found to be comparable with those recorded previously [26, 27]. Values of $\overline{E}_c$ obtained for the two phases $PbSe_2$ and PbSe when crystallized from the annealed glasses were found to be relatively smaller than those estimated when the same phases were crystallized from as-prepared glasses. This discrepancy can be attributed to formation of nuclei sites in the annealed glasses; that is the activation energy of crystallization of the phases crystallized from annealed glasses are representative of the growth process.

Conclusions

The results of DSC and XRD emphasized that the investigated $Pb_{20}Ge_{17}Se_{63}$ and $Pb_{20}Ge_{22}Se_{58}$ glasses are crystallized to $GeSe_2$ and $PbSe_2$ as well as $GeSe_2$ and PbSe, respectively. The variations of T_g with $\ln\phi$ observed for $Pb_{20}Ge_{17}Se_{63}$ and $Pb_{20}Ge_{22}Se_{58}$ glasses indicate different structural changes at glass transition regions, as a result of partial destruction of the glassy matrix network. The activation energy for glass transition (E_t) was calculated.

The activation energy of crystallization E_c of the different observed phases was calculated using Kissinger, Augis–Bennett and modified JMA equations. The calculations revealed the agreement of the results obtained by the methods of Kissinger and Augis–Bennett, and the respective obvious difference between them and those obtained on the basis of JMA equation may be attributed to the applicability of JMA equation to non-isothermal kinetics of the two glasses investigated.

It was found that $GeSe_2$ could be crystallized by surface crystallization and the two phases $PbSe_2$ and PbSe by bulk crystallization in three dimensions. Besides, the annealing process of the investigated glasses affects greatly their thermal parameters.

* * *

The author is grateful to Prof. M. M. Ibrahim and Dr. E. Kh. Shokr for their helpful discussions. Also, thanks to Dr. Angela B. Seddon for her kind assistance in this work during my visit to the School of Materials, University of Sheffield, UK.

References

1 J. A. Savage, Infrared optical materials and their antireflection coatings, Adam Hiliger, Bristol 1985.
2 Z. Cimpl and F. Kosek, J. Non-Cryst. Solids, 90 (1987) 577.
3 A. B. Seddon and M. J. Laine, J. Non-Cryst. Solids, 213 (1997) 168.
4 N. F. Mott, E. A. Davis and R. Street, Phil. Mag., 32 (1975) 961.

5 N. Tohge, T. Minami, Y. Yamamoto and M. Tanaka, J. Appl. Phys., 51 (1980) 1048.
6 N. Tohge, H. Matsuo and T. Minami, J. Non-Cryst. Solids, 95–96 (1987) 809.
7 K. L. Bhatia, S. K. Malik, N. Kishore and S. P. Singh, Phil. Mag. B, 66 (1992) 587.
8 B. Vaidhyanathan, S. Murugavel, S. Asokan and K. J. Rao, J. Physical Chemistry B., 101 (1997) 9717.
9 D. W. Handerson, J. Non-Cryst. Solids, 30 (1979) 301.
10 M. F. Kotkata and E. A. Mahmoud, Mater. Sci. Engin., 54 (1982) 163.
11 H. Yinnon and D. R. Uhlmann, J. Non-Cryst. Solids, 54 (1983) 253.
12 H. E. Kissinger, J. Res. Nat. Bur. Stand, 57 (1956) 217; idem, Anal. Chem., 29 (1957) 1702.
13 J. A. Augis and J. E. Bennett, J. Thermal Anal., 13 (1978) 283.
14 K. Matusita, T. Komatsu and R. Yokota, J. Mater. Sci., 19 (1984) 291.
15 K. Tanaka, Phys. Rev. B, 39 (1989) 1270.
16 L. Pauling, The Chemical Bond, Cornell University, New York 1976.
17 R. T. Sanderson, The Chemical Bonds and Bonds Energy, Academic Press, New York 1976.
18 L. Tichy and H. Ticha, J. Non-Cryst. Solids, 189 (1995) 141.
19 M. Lasocka, Mat. Sci. Eng., 23 (1976) 173.
20 J. Colemenero and J. M. Barandiaran, J. Non-Cryst. Solids, 30 (1978) 263.
21 S. Mahadevan, A. Giridhar and A. K. Singh, J. Non-Cryst. Solids, 88 (1986) 11.
22 A. Hruby and L. Stourac, Mat. Res. Bull., 6 (1971) 465.
23 K. Matusita and S. Sakka, Phys. Chem. Glasses, 20 (1979) 81.
24 J. Malek, Thermochim. Acta, 267 (1995) 61.
25 R. F. Speyer and S. H. Risbud, Phys. Chem. Glasses, 24 (1983) 26.
26 M. D. Baro, M. T. Clavaguera-Mora and N. Clavaguera, J. Mater. Sci., 19 (1984) 3005.
27 N. Afify, J. Non-Cryst. Solids, 126 (1990) 130.